Meteorites
2, Nos. 1–2, 2012, 15–30
www.meteorites.pwr.wroc.pl
DOI 10.5277/met120103

SOŁTMANY METEORITE

Łukasz KARWOWSKI[1]

[1] University of Silesia, Faculty of Earth Sciences, Department of Geochemistry, Mineralogy and Petrology; ul. Będzińska 60, 41-200 Sosnowiec, Poland

Abstract: This paper presents the results of a mineralogical and petrological study of the Sołtmany meteorite, which fell on April 30, 2011 in northern Poland. The meteorite was found almost immediately after it fell and has been little altered by weathering. Sołtmany is not the only observed fall of an L6 chondrite over Europe in the past few years. The preceding fall of this type, Jesenice (Slovenia), was also witnessed in April of 2009. However, it was not until several weeks after the fall that the first specimen of Jesenice was found, whereas Sołtmany was collected after a few minutes and submitted for analysis within a couple of days.
The author presents mineral and petrographic features and chemical characteristics of mineral phases in Sołtmany. The mineral components are represented by metallic phases (kamacite, taenite, tetrataenite, native copper), as well as chromite, olivine, low- and high-calcium pyroxene, feldspar, chlorine-bearing apatite, and merrillite. This study also describes the texture of the meteorite and takes notice of a low number of preserved chondrules and the presence of oval chondrule-like areas, which exhibit a metamorphosed, recrystallized texture. Sołtmany was classified as an L6 ordinary chondrite with a weathering grade of W0. A shock stage S2 was determined on the basis of undulose extinction and lack of planar fractures in olivine crystals.

Keywords: meteorite, ordinary chondrite, L6 chondrite, meteorite fall, hammer meteorite, Warmińsko-Mazurskie Province, Sołtmany village

INTRODUCTION

The meteorite fell on April 30, 2011 at 6:03 am (CEST) on the farm of Mrs. Alfreda Lewandowska in Sołtmany. The village is located in the Warmińsko-Mazurskie Province in northern Poland. The exact coordinates of the fall location are 54°00.53'N, 22°00.30'E. The meteorite punched a hole through the roof and hit the concrete steps leading to a farm building. The hole in the roof and the marks left in concrete suggest that the fall's final trajectory was nearly perpendicular to the Earth's surface. The circumstances of the fall and its recovery are described in detail in the introductory article to this volume of *Meteorites* (Woźniak & Woźniak, 2012).

The total known weight of Sołtmany was determined to be approximately 1066 g. Upon impact, the meteorite broke into two large pieces of 813 g and 155 g respectively, as well as numerous smaller fragments. A type specimen of 65 grams is held by the Faculty of Earth Sciences of the University of Silesia in Sosnowiec, Poland. A larger fragment of 120 grams is in possession of the Faculty of Geoengineering, Mining and Geology of the Wrocław University of Technology.

The previous witnessed fall of an L ordinary chondrite in Europe also took place in April. The event was witnessed on April 9, 2009 at 3:00 am (CEST) in Slovenia, near the Austrian border. The resulting meteorite was given the name of Jesenice and was classified as an ordinary chondrite of petrologic type L6 with a shock stage S3. Three stones comprising the weight of 3.611 kg were found within several weeks after the fall (Bischoff et al., 2011).

Corresponding author: Łukasz KARWOWSKI, lukasz.karwowski@us.edu.pl

MATERIAL AND METHODS

The macroscopic texture of Sołtmany is uniform and unbrecciated. The macrophotographs of the meteorite as well as the photographs of four fragments dedicated for research were presented by Woźniak & Woźniak (2012). The material for analysis consisted of two small fragments, being representative for the whole mass of the meteorite, four polished thin sections, and several specks partially covered with fusion crust. The meteorite was studied by means of optical microscopy in transmitted and reflected light. The specimens were also documented photographically. The quantitative analysis was performed by means of an electron microscope CAMECA SX-100, at the Laboratory of Microanalysis of Minerals and Synthetic Substances at the Faculty of Geology of Warsaw University. Further analysis of the fusion crust was conducted with a scanning electron microscope XL 30 ESEM-TMP PHILLIPS equipped with the EDAX analytical device at the Faculty of Earth Sciences of the University of Silesia in Sosnowiec.

FUSION CRUST

Sołtmany is covered with a black, dark-brownish, and somewhat shiny fusion crust. As a result of its impact into the asbestos cement roof board and timber, scraps of construction materials are embedded into the fusion crust on some surfaces. Numerous fibers of chrysotile asbestos were identified among other materials. The surface texture of the crust is slightly rough, and it exhibits small vesicles. Under a magnifying glass, it is shiny and glassy. The thickness of the fusion crust was measured on cut sections and it varies slightly from 0.5 to 0.7 mm.

The scanning electron microscope image revealed additional characteristics of the fusion crust. It is highly textured, with close-grained vesicles set in between abundant protuberances (Fig. 1).

The vesicles are largely filled with the construction material from the asbestos cement board and meteoritic material from both the inside and outside of the meteorite. The observations were made on the surface of fragments of the fusion crust collected from the concrete floor where the meteorite had landed. The characteristics and composition of the vesicles can be best observed on cut cross sections of the fusion crust (Fig. 2).

It can be inferred that the vesicles represent the places where gases expanded during solidification of the fusion crust. The vesicles are connected to the remnants of gas bubbles inside of the fusion crust. Their shapes attest to their origin in liquid state during ablation of the surface of the meteoroid. The remnants of gas bubbles expand as deep as 50–60 μm into the fusion crust.

At larger magnification the rock reveals indistinct, densely-arranged dendritic crystals of spinel on the external surface of the fusion crust. The thin and long dendrite forms are mainly composed of iron, nickel and magnesium. The thicker and smaller dendrites, which take isometric forms, are rich in Fe, Cr, and Mg (Fig. 3). They likely match the chemical composition of chromite, yet, unlike the thin and long spinels, they are present only locally. Certain remnants of gas bubbles also contain dendritic crystals of a mineral that is similar in chemical composition to a nickel-iron spinel (trevorite). Unfortunately, a plausible explanation for its origin in the gas bubbles cannot be provided (Fig. 4).

In transmitted light, the fusion crust is mostly opaque or dark brown and semi-translucent. Narrow translucent areas composed of pyroxene and olivine grains are scattered throughout the fusion crust.

The electron microscopic examination of the fusion crust revealed three different parts (Fig. 5). The first part is the outermost layer and it is glassy and heterogeneous in texture. Locally, it is visibly rich in iron and magnesium. In other areas, it is equivalent in chemical composition to feldspathic glass and is enriched in alkali elements (Na, Ca, K), aluminum oxide, and silica. This external layer exhibits abundant pores and remnants of gas bubbles (mostly of volatile sulfur compounds). It is opaque in transmitted light due to the oxidized iron content (magnetite-bearing Ni), and other opaque mineral phases (mostly spinels).

The second layer of the fusion crust is partially transparent (to transmitted light) and it is thoroughly melted. The feldspar in the outermost part of the meteorite was the main fusing agent while ablation was taking place. The product of the softening process is strongly vitrified or isotropized that is a result of having reached the softening point of feldspar. It seems that the temperature reached by this layer was slightly above 1250 °C. Feldspar was completely vitrified or isotropized; pyroxene and olivine began to melt at the points of contact with feldspar glass (Fig. 6).

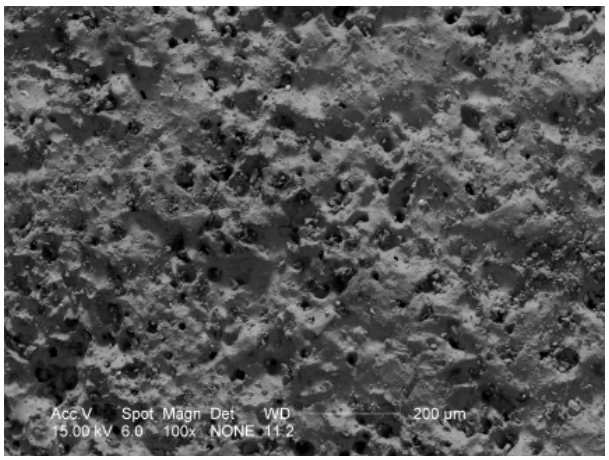

Fig. 1. Surface of the fusion crust. Numerous cavities can be observed. Some of the cavities are secondarily filled with µm-sized grains of both the construction material and the meteorite. SEM (mixed SE/BSE image)

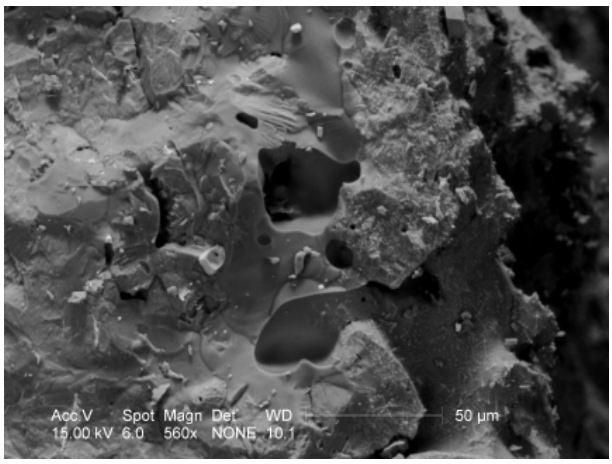

Fig. 2. A cross section through the fusion crust. Note a vesicle connected with the remnant of a gas bubble. SEM (mixed SE/BSE image)

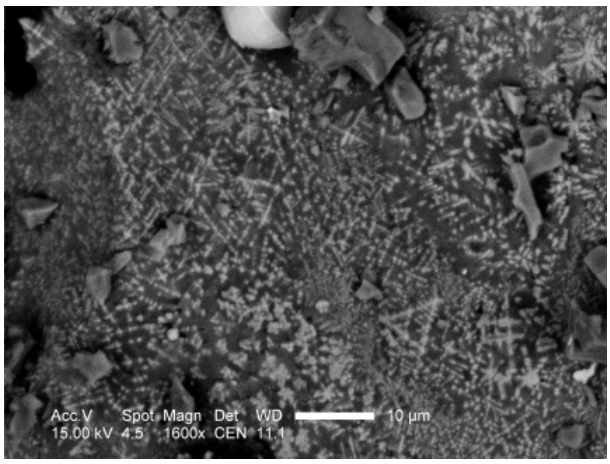

Fig. 3. Spinels on the surface of the fusion crust. Thin, skeletal spinels are composed of Fe, Ni, and Mg. Somewhat more isometric depositions on the lower left-hand side of the image represent chromite spinels. SEM (mixed SE/BSE image)

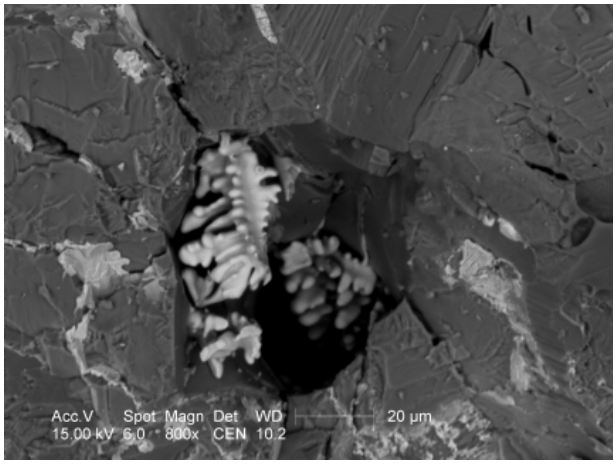

Fig. 4. Dendritic crystals consistent with the chemical composition of iron-nickel spinel (trevorite-type) in a cavity. SEM (mixed SE/BSE image)

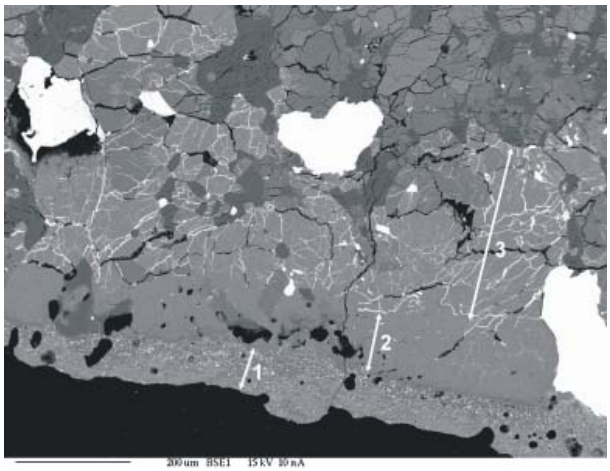

Fig. 5. Stratified fusion crust. The outer glassy layer contains spinels (1). The next layer exhibits partially melted olivines and pyroxenes and melted feldspar (2). Abundant, thin, µm-sized veins of iron sulfide are a characteristic feature of the innermost layer, termed "black veins" in this study (3). SEM (BSE image)

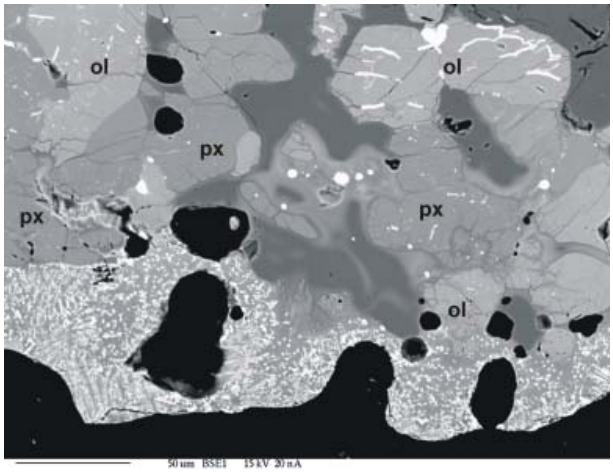

Fig. 6. Strongly melted layer of fusion crust with fragments of partially melted olivines (ol) and pyroxenes (px). The glassy fusion crust with µm-sized crystals of spinel can be observed at the bottom of the image. The upper part of the image shows the transitional zone to the "black veins" zone. SEM (BSE image)

The third layer of the fusion crust is a so called "layer of black veins". It is composed of fractured minerals of the meteorite. The cracks are filled with a sulfide (similar in composition to troilite) and metallic alloys. The cracks are so numerous that they appear to constitute a layer that is opaque to transmitted light. The so called "black veins" were observed in all silicates in the meteorite excluding feldspar grains. The thermal softening of feldspar at high temperatures is responsible for the lack of "black veins" in feldspar. The same heating cracked olivine and pyroxene crystals (Fig. 7). The cracks were secondarily filled by low-viscosity sulfide.

In transmitted light, the fusion crust is almost opaque, but in some places the same fusion crust appears to be a slightly translucent layer. Analytical studies using SEM-EDX demonstrate that the composition of the vitrified fusion crust is heterogeneous and is subject to variation, especially in Mg, Fe, and Al content. The glass is primarily feldspathic. Nevertheless, outer, homogenous, glassy fragments of the fusion crust, which show neither the effects of crystallization, nor contain spinels, were also locally encountered (Fig. 8). They probably represent the last drops of glass, solidified in the final stages of ablation, which are similar in composition to feldspar with a significant admixture of iron. The fusion crust, however, primarily contains numerous dendritic crystals of spinel rich in iron, nickel and magnesium (Fig. 9).

The glassy layer smoothly turns into the next layer which is translucent in places. The amount of glass decreases towards the inside of the meteorite, that is, the zone of "black veins", and gives place to isotropized grains of feldspars. Olivines and pyroxenes are only

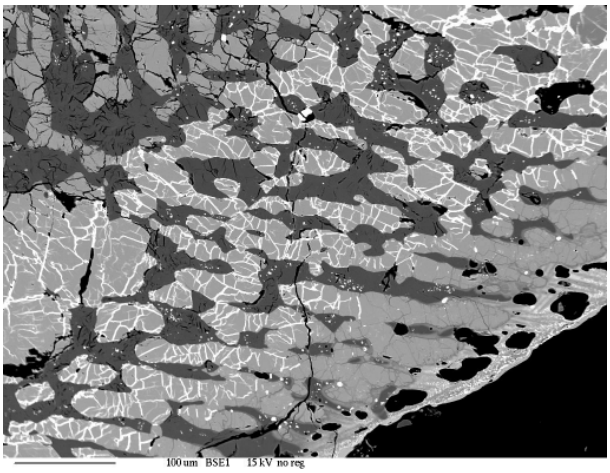

Fig. 7. The layer of "black veins" present at the margin of an olivine-rich chondrule. Sulfide veins are present in the olivine. Feldspar is devoid of FeS veins. A very thin layer of glassy fusion crust can be seen in the lower right corner. SEM (BSE image)

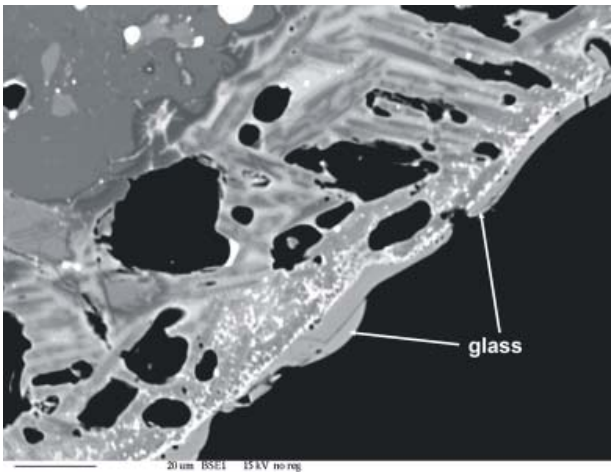

Fig. 8. The outermost layers of the fusion crust are homogenous and devoid of spinel microcrystals (glass). Remnants of gas bubbles are present and an area of partial melting can be observed in the upper right-hand part of the image. SEM (BSE image)

Fig. 9. Minor FeNi-metal within a grain of troilite. SEM (BSE image)

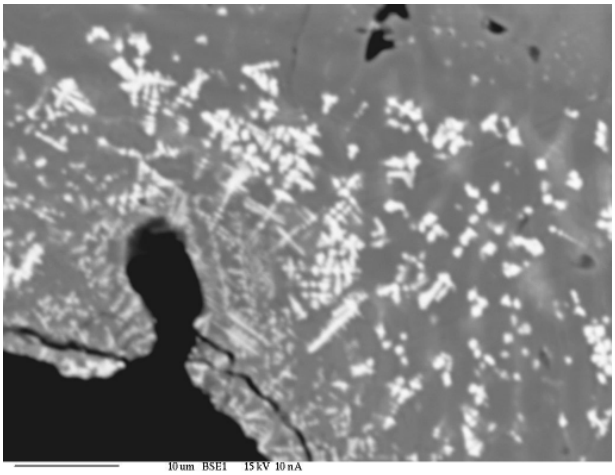

Fig. 10. Dendritic Fe-Ni-Mg spinels in a glassy area of the fusion crust. SEM (BSE image)

slightly melted (Fig. 6). Grains of troilite in this area are partially decomposed and contains zones where admixed iron is present (Fig. 9). The chemical composition of the troilite is variable. Some of the troilites contain up to approximately 1% Ni (Tab. 1).

The chemical composition of the feldspar glass varies locally and depends on the surrounding coherent minerals. The fusion crust is visibly thinner in places with metamorphosed, recrystallized textures, which are rich in pyroxene and poor in feldspar, as well as olivine crystals (Fig. 7). Small bulges on the surface are very often present in these places.

Dendritic spinels are commonly observed in the fusion crust (Figs. 3 and 10). Their chemical composition varies from that of magnetite to trevorite, as well as chromite. Due to their minute sizes, exact quantitative chemical analyses were not feasible. Only a qualitative analysis could be performed.

Although sparse, relict grains of chromite, belonging to the least fusible minerals of the meteorite, were identified in the external part of the fusion crust. An increase in chromium content was observed around chromite grains in the partially recrystallized area of the glassy fusion crust. They are less abundant in this area, but unoxidized sulfide and metallic grains occur as well. Their chemical composition can be found in Tab. 2. The metallic grains are mainly taenite and, less often, kamacite (Tab. 2, pos. 4, 5, 6 and 7). The grains rich in sulfur have a peculiar chemical composition. In some cases they are compositionally similar to pentlandite, but typically they have a non-stoichiometric behavior (Tab. 2, pos. 1, 2 and 3).

Based on the thickness of the fusion crust, it can be argued that the flight of the meteoroid through the Earth's atmosphere was relatively short in duration. The meteoroid must have tumbled, as the main mass of Sołtmany does not show the characteristics of "orientation". The meteorite might have separated from a larger body at a relatively low altitude. The character of the fusion crust and its thickness which does not exceed 0.7 mm may attest to its secondary origin. Consequently, it can be inferred that further fragments of the meteorite might yet be found. Nevertheless, they are likely scattered over a wide area.

Table 1. Chemical composition of Ni-rich sulfides (troilite) from the melting zone of fusion crust. Results in wt.%.

	S18	S19	S20	S21
Si	0.01	nd	nd	nd
P	nd	nd	nd	nd
S	36.67	36.68	36.67	36.69
Fe	62.48	62.49	62.41	62.48
Ni	1.58	1.52	1.51	1.57
Co	0.19	0.17	0.18	0.18
Total	100.93	100.86	100.77	100.92
at.%.				
Si	0.01	–	–	–
P	–	–	–	–
S	49.88	49.91	49.94	49.90
Fe	48.80	48.83	48.80	48.80
Ni	1.18	1.13	1.12	1.17
Co	0.14	0.13	0.13	0.13
Total	100.00	100.00	100.00	100.00

nd – not detected

Table 2. Chemical composition of non-stoichiometric sulfide (1-3) and metallic phases (4-7) in the fusion crust. Results in wt.%.

	1.	2.	3.	4.	5.	6.	7.
Si	0.06	0.14	0.02	0.01	nd	nd	nd
P	nd	0.01	nd	0.01	nd	nd	0.01
S	25.37	6.99	25.66	nd	nd	0.01	0.01
Fe	3.37	90.05	64.98	71.97	94.50	93.94	64.07
Ni	71.56	2.34	8.70	27.93	6.11	6.02	36.50
Co	nd	0.28	0.24	0.27	0.96	0.76	0.25
Total	100.36	99.81	99.60	100.19	101.57	100.73	100.84
at.%							
Si	0.11	0.27	0.03	0.01	–	–	–
P	–	0.02	–	0.02	–	–	0.01
S	38.17	11.59	37.80	–	–	0.02	0.01
Fe	2.91	85.76	54.97	72.82	93.36	93.56	64.68
Ni	58.80	2.12	7.00	26.89	5.74	5.70	35.05
Co	–	0.25	0.19	0.26	0.89	0.72	0.24
Total	100.00	100.00	100.00	100.00	100.00	100.00	100.00

nd – not detected

METEORITE CHARACTERISTICS

The meteorite was macroscopically fresh a few days after the fall and exhibited exceptionally white interior with delicate tones of gray. After a few months, the surfaces that were not covered with fusion crust became visibly darker. Tiny rust spots appeared around the metallic grains of fragments that had been exposed to water during cutting. Initial observations under a binocular loupe led to the conclusion that the meteorite is a chondrite. Low metal abundances, but abundant troilite suggest a classification of L or LL group. Tiny metallic phases are sparsely distributed throughout the stone's light-coloured matrix. A number of rounded objects in the mm size-range were identified, resembling large chondrules at a cursory glance. Additional observations proved that they represent metamorphosed, recrystallized chondrules surrounded by tiny troilite grains. In thin sections, the clear identification of a number of relict chondrules is possible, proving conclusively that Sołtmany is a chondrite.

Opaque minerals

Chemical microanalyses and microscopic observations in reflected light enabled the identification of opaque minerals. The main opaque phase is troilite. The metallic phases (kamacite and taenite) are also rarely accompanied by troilite (Figs. 11b,c), which seldom reaches more than a few mm in diameter. The chemical microanalyses led to the conclusion that the troilite had few measurable impurities (Tab. 3). Troilite inclusions over 2 mm in diameter are relatively sparse in the meteorite. More often, tiny grains of troilite constitute rims around recrystallized chondrules and mineral fragments.

Taenite and kamacite are the most abundant metallic phases. They sometimes coexist within grains (Figs. 11a,d) or form plessite (Figs. 11a,b). In plessite intergrowths, the kamacite is extremely poor in nickel (2.77 at.%), whereas the average nickel content

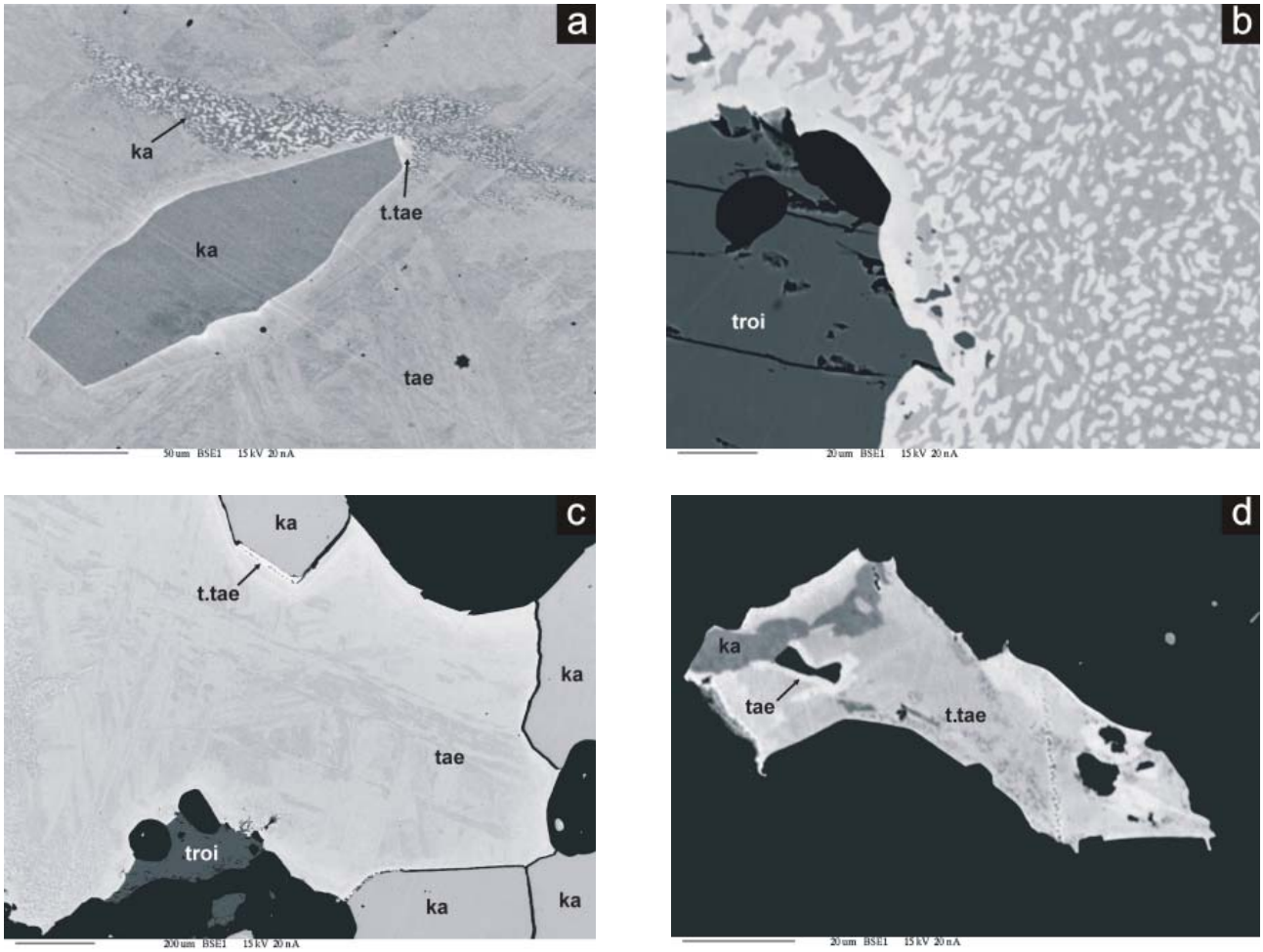

Fig. 11. Opaque minerals: **a** – grain of kamacite (ka) surrounded by lamellar taenite (tae); a (tetrataenite) rim on the kamacite-taenite boundary (t.tae); grain of plessite can be observed at the top of the image; **b** – plessite; Ni-poor kamacite in plessite; also visible is a grain of troilite (troi); **c** – taenite (tae) of lamellar texture surrounded by kamacite grains (ka) and troilite (troi); tetrataenite at the kamacite-taenite boundary (t.tae); **d** –taenite (tae) exhibiting a blotchy paragenesis with kamacite (ka) and tetrataenite grains (t.tae); all BSE images

Table 3. Chemical composition of troilite grains. The chemical formula was calculated for $S_{\Sigma=1}$. Results in wt.%.

	12	13	14	15a	16a
Fe	64.43	64.27	65.04	64.14	64.07
Ni	0.01	nd	nd	nd	nd
Co	nd	nd	nd	nd	nd
Mn	0.03	0.14	0.05	0.05	0.12
Ti	nd	0.02	0.01	0.05	0.01
Cr	nd	nd	0.01	0.01	nd
Cu	nd	nd	nd	nd	nd
S	36.78	36.59	36.65	35.95	36.29
Total	101.25	101.02	101.76	100.20	100.49
at.%					
Fe^{2+}	1.01	1.01	1.02	1.02	1.01
Ni^{2+}	< 0.01	–	–	–	–
Co^{2+}	–	–	–	–	–
Mn^{2+}	< 0.01	< 0.01	< 0.01	< 0.01	< 0.01
Ti^{4+}	–	< 0.01	< 0.01	< 0.01	< 0.01
Cr^{3+}	–	–	< 0.01	< 0.01	–
Cu^{2+}	–	–	–	–	–
S^{2-}	1.00	1.00	1.00	1.00	1.00
Total	2.01	2.01	2.02	2.02	2.02

nd – not detected

is slightly below 6 at.%. The kamacite contains a high Co content (from 0.61 to 0.99 at.%) with an average Co content of 0.7 at.% (Fig. 12). The high nickel phases contain significantly less Co.

Kamacite often forms individual grains distinct from taenite (Fig. 11c). The grains of taenite are vary from 16 to 37 at.% Ni. The taenite is heterogeneous. The taenite grains contain regions of plessite with higher Ni content than the surrounding areas (Figs. 11a,c). High-Ni phase, which is considered to be tetrataenite, was identified at the boundaries of kamacite and taenite grains (Figs. 11a,c, 13). The variability of the Ni to Fe ratio in the metallic phases is depicted in

Table 4. Chemical composition of Cu grains. Results in wt.%.

	1	2	3
Cu	95.83	94.72	95.01
Ni	1.89	1.90	1.86
Fe	3.52	3.44	3.51
Co	nd	nd	nd
Total	101.24	100.06	100.38
at.%			
Cu	94.06	94.07	94.08
Ni	2.01	2.05	2.04
Fe	3.93	3.89	3.88
Co	–	–	–
Total	100.00	100.00	100.00

nd – not detected

Fig. 13. Fields of kamacite, taenite, and tetrataenite are included on the diagram. The isolated intermediate values likely correspond to data gathered at phase or grain boundaries, which exhibit extremely variable nickel content. Such mineral associations of various FeNi phases are characteristic of metamorphic conditions and are typically associated with petrologic type 5 and 6, L and H ordinary chondrites (Reisener & Goldstein, 2003).

Metallic copper is present, mostly within taenite grains. However, small inclusions of Cu within kamacite grains and single grains within troilite inclusions were also identified. All of the Cu grains are homogenous. They contain ~2 at.% Ni and ~3.9 at.% Fe (Tab. 4).

Spinel identified as chromite is the last of the found opaque minerals. It occurs as small grains embedded within the silicate matrix. Inclusions of chromite within chondrules were also identified; however, these were smaller and unevenly distributed. Emulsion-type depositions of chromite were also quite abundant within chondrule feldspars (Fig. 14). The chemical

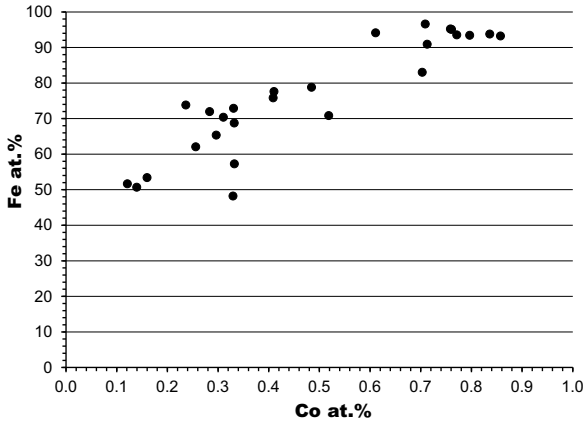

Fig. 12. Correlation of Fe and Co content in the metallic phases of Sołtmany

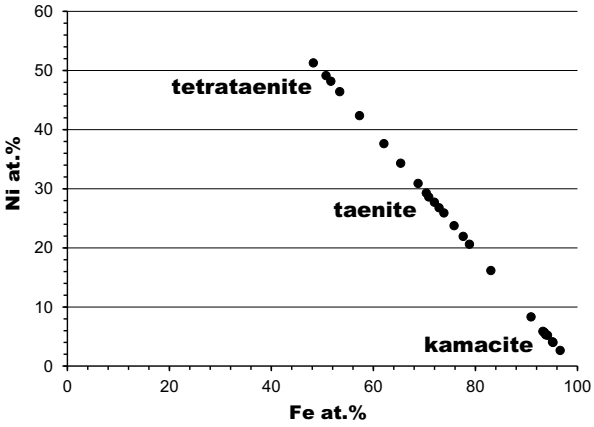

Fig. 13. Correlation of Ni and Fe content in the metallic phases of Sołtmany

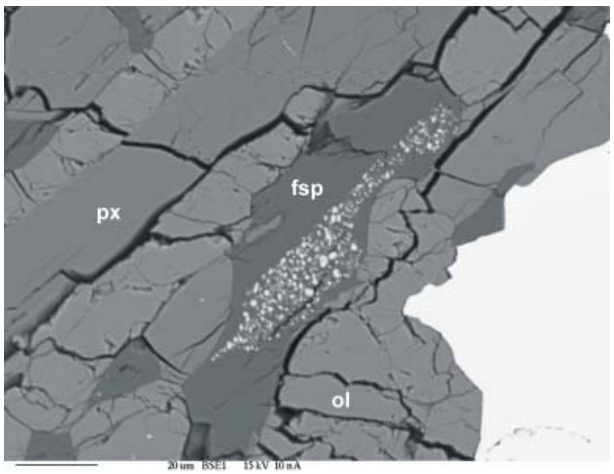

Fig. 14. Emulsion-type depositions of chromite (light spots) in feldspar (fsp). A fragment of a porphyritic olivine (ol) – pyroxene (px) chondrule (POP). FeNi-metal is visible in the lower right-hand corner of the image. SEM (BSE image)

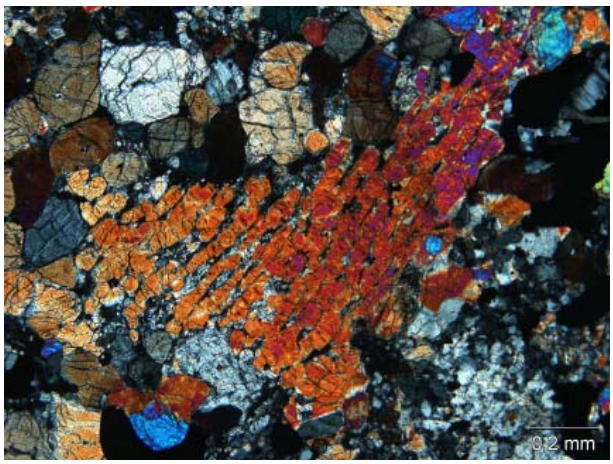

Fig. 15. Fragment of an olivine-rich relict chondrule embedded in the recrystallized matrix. Transmitted light, crossed nicols

composition of these chromites corresponds to that of the larger inclusions. The chemical composition of selected grains of chromite can be found in Tab. 5. They are clearly enriched in Ti and Al.

Silicates

Chondrules account for a small percentage of the volume of the meteorite. They are mostly incomplete and lack characteristic rimming. Chondrule fragments are

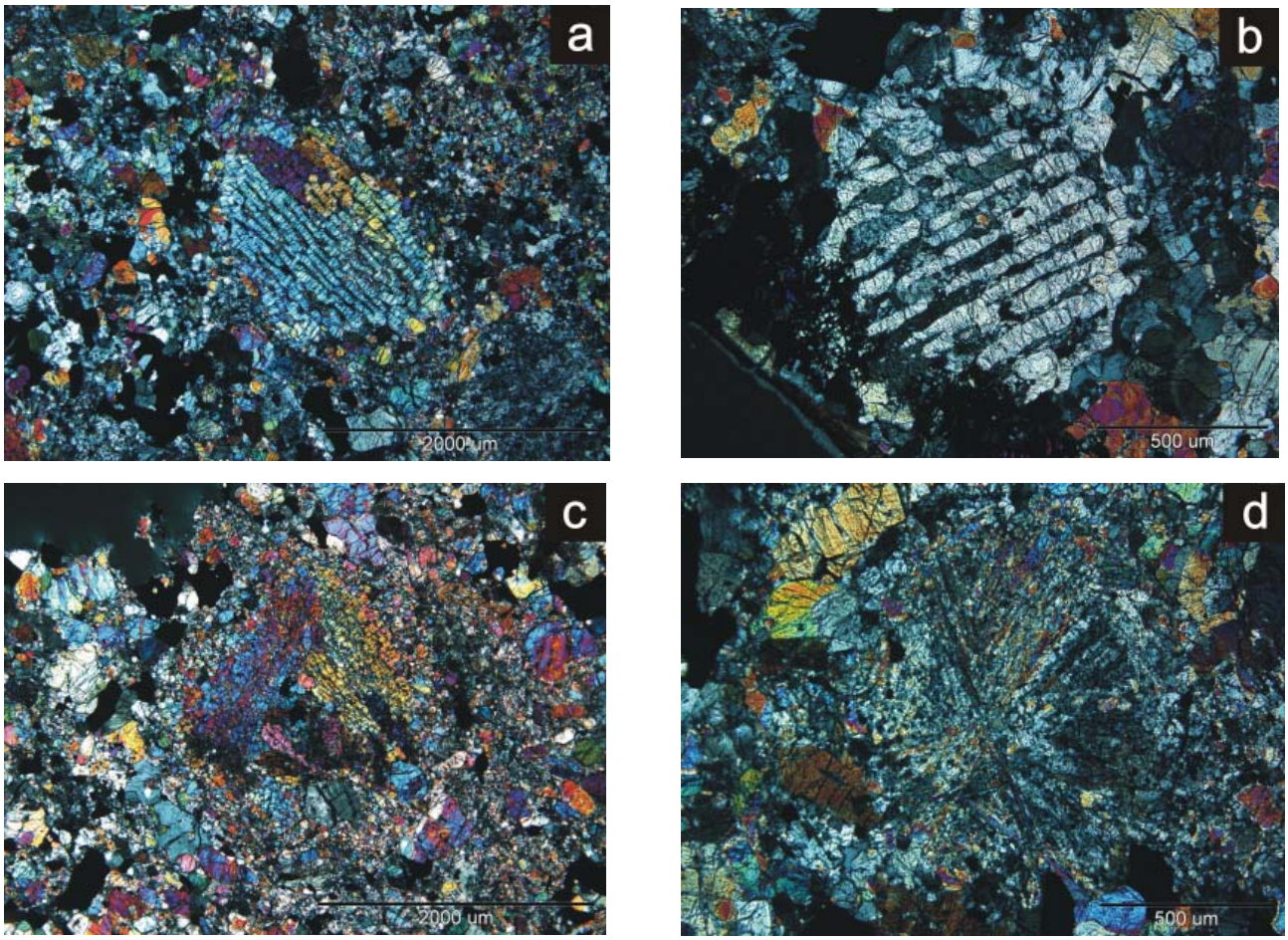

Fig. 16. Relict chondrules and chondrule-like areas of metamorphosed, recrystallized material in Sołtmany: **a** – barred-olivine chondrule (BO) surrounded by recrystallized matrix; **b** – barred-olivine chondrule (BO) on the edge of a thin section; note the anisotropy of feldspar (plag); **c** – chondrule-like recrystallized area composed of olivine, pyroxene, and plagioclase; **d** – radial, chondrule-like object of pyroxene and olivine, this is probably the relict of a former radial pyroxene (RP) chondrule; all images in transmitted light, crossed nicols

Table 5. Chemical composition of chromite-type spinels. Results in wt.%. Chemical formula calculated according to $4O^{2-}$. Total sum of cations is 3

	1.	2.	S-5	S-6	S-7	Schr1.	Schr.2
SiO_2	nd	nd	nd	0.02	nd	nd	nd
TiO_2	3.13	3.19	2.73	3.12	2.81	3.13	3.19
Al_2O_3	5.51	5.46	5.78	5.52	5.93	5.51	5.46
V_2O_3	nd	nd	0.79	0.74	0.87	nd	nd
Cr_2O_3	55.66	56.18	54.40	55.02	55.26	55.66	56.18
Fe_2O_3	3.42	3.06	3.86	3.27	3.20	3.42	3.06
MgO	2.64	2.76	2.27	2.50	2.26	2.64	2.76
CaO	nd	nd	0.01	nd	nd	nd	nd
MnO	0.63	0.81	0.80	0.62	0.68	0.63	0.81
FeO	27.51	27.26	27.91	27.81	28.40	27.51	27.26
CoO	nd	nd	0.02	nd	0.05	nd	nd
NiO	nd	nd	0.03	nd	nd	nd	nd
ZnO	0.33	0.22	0.28	0.22	0.21	0.33	0.22
Total	98.83	98.94	98.88	98.84	99.67	98.83	98.94
at. %							
Si^{4+}	–	–	–	< 0.01	–	–	–
Ti^{4+}	0.08	0.08	0.07	0.08	0.07	0.08	0.08
Al^{3+}	0.23	0.23	0.24	0.23	0.25	0.23	0.23
V^{3+}	–	–	0.02	0.02	0.02	–	–
Cr^{3+}	1.57	1.58	1.54	1.55	1.55	1.57	1.58
Fe^{3+}	0.09	0.08	0.10	0.09	0.08	0.09	0.08
Mg^{2+}	0.14	0.15	0.12	0.13	0.12	0.14	0.15
Ca^{2+}	–	–	< 0.01	–	–	–	–
Mn^{2+}	0.02	0.02	0.02	0.02	0.02	0.02	0.02
Fe^{2+}	0.82	0.81	0.83	0.83	0.84	0.82	0.81
Co^{2+}	–	–	< 0.01	–	< 0.01	–	–
Ni^{2+}	–	–	< 0.01	–	–	–	–
Zn^{2+}	0.01	0.01	0.01	0.01	0.01	0.01	0.01
Total	2.97	2.97	2.97	2.97	2.97	2.97	2.97

nd – not detected

also common (Fig. 15). Fan-shaped radial pyroxene chondrules (RP) were not identified.

Olivine-rich chondrules containing recrystallized small grains of plagioclase were the easiest to discern (Figs. 16a,b).

Chondrule-like accumulations of metamorphosed, recrystallized olivine and pyroxene (relict chondrules) are common (Figs. 16c,d). Grains with a peculiar texture occur in the vicinity of chondrules (Figs. 17a,b). The majority of the meteorite is composed of a mass that is recrystallized in texture, contains grains of variable size, and does not cantain chondrules (Fig. 18). Certain fragments are recrystallized and are very fine-grained.

The silicate phases are represented by low-Ca pyroxene (hypersthene), Ca-pyroxene, olivine, and feldspar, both inside and outside of the chondrules. The variability in the chemical composition of respective minerals can be found in Tables 6 and 7. The analyses did not reveal any major variability in the chemical composition of pyroxenes in any constituents of the rock (e.g., chondrules, chondrule fragments, or silicate-rich areas having a metamorphosed, recrystallized texture). The whole rock appears to have a common, metamorphic origin. The chemical variability of the low-calcium pyroxenes is minimal. The average Fs content is 21.4 mol%. Fs varies between 21.02 and 21.91 mol%. High-Ca pyroxenes are similar in composition to diopsides, with Wo content between 44.23 and 46.28 mol% with an average of 45.3 mol%.

Olivines are also well equilibrated in this meteorite. No major variation in the chemical composition was observed between olivine from chondrules, recrystallized areas, and the matrix (Tab. 8). Fa content ranges slightly from 24.72 to 25.89 mol%, with an average of 25.5 mol%.

Minor amounts of feldspar are present in all silicates. It is present as plagioclase (oligoclase), rich in orthoclase component (Or: 4.65–7.86 mol%; Tab. 9). There is also no significant variation in the chemical composition of the feldspar. Plagioclase often occurs in higher abundances around certain metamorphosed, recrystallized areas (Fig. 19).

Table 6. Chemical composition of representative low-Ca pyroxenes. Results in wt.%. Chemical formula calculated according to $6O^{2-}$

	#1	#5	#7	#8	So4.ch	So7.ch	So8.	So14.	So16.	So18.	So20.	19. ch	24	28	29
SiO_2	55.85	55.79	55.96	55.63	55.94	55.67	56.00	55.65	55.91	55.72	55.66	55.85	55.79	55.96	55.63
TiO_2	0.19	0.20	0.21	0.23	0.15	0.17	0.16	0.23	0.18	0.18	0.21	0.19	0.20	0.21	0.23
Al_2O_3	0.12	0.13	0.12	0.16	0.13	0.16	0.09	0.14	0.13	0.13	0.14	0.12	0.13	0.12	0.16
V_2O_3	nd	nd	nd	nd	0.07	nd	0.07	0.05	0.01	nd	0.03	nd	nd	nd	nd
Cr_2O_3	0.09	0.09	0.08	0.14	0.10	0.18	0.14	0.14	0.13	0.09	0.10	0.09	0.09	0.08	0.14
Fe_2O_3	0.05	nd	nd	0.57	nd	0.19	nd	0.26	nd	0.30	nd	0.05	nd	nd	0.57
FeO	14.37	14.12	14.16	13.91	14.12	14.12	14.17	14.45	13.94	14.06	14.46	14.37	14.11	14.16	13.91
MnO	0.50	0.51	0.53	0.54	0.45	0.51	0.48	0.40	0.49	0.50	0.25	0.50	0.51	0.53	0.54
CaO	0.70	0.73	0.71	0.96	0.81	0.77	0.71	0.78	0.68	0.75	0.77	0.70	0.73	0.71	0.96
MgO	28.71	28.62	28.68	28.62	28.58	28.66	28.58	28.54	28.87	28.75	28.36	28.71	28.61	28.68	28.62
Na_2O	nd	nd	nd	nd	nd	nd	0.01	nd	0.02	nd	nd	nd	nd	nd	nd
K_2O	nd	nd	nd	0.01	nd	nd	nd	nd	0.01	nd	nd	nd	nd	nd	0.01
NiO	nd	nd	nd	nd	0.07	nd	0.06	nd	nd	nd	nd	nd	nd	nd	nd
Total	100.58	100.19	100.45	100.77	100.42	100.43	100.47	100.64	100.37	100.48	99.98	100.58	100.17	100.45	100.77
at.%															
Si^{4+}	1.990	1.993	1.994	1.981	1.995	1.987	1.996	1.985	1.993	1.987	1.994	1.990	1.993	1.994	1.981
Ti^{4+}	0.005	0.005	0.006	0.006	0.004	0.005	0.004	0.006	0.005	0.005	0.006	0.005	0.005	0.006	0.006
Al^{3+}	0.005	0.006	0.005	0.007	0.006	0.007	0.004	0.006	0.006	0.005	0.006	0.005	0.006	0.005	0.007
V^{3+}	–	–	–	–	0.002	–	0.002	0.001	< 0.001	–	0.001	–	–	–	–
Cr^{3+}	0.002	0.003	0.002	0.004	0.003	0.005	0.004	0.004	0.004	0.003	0.003	0.002	0.003	0.002	0.004
Fe^{3+}	0.001	–	–	0.008	–	0.003	–	0.004	–	0.004	–	0.001	–	–	0.008
Fe^{2+}	0.428	0.422	0.422	0.414	0.421	0.422	0.422	0.431	0.415	0.419	0.433	0.428	0.422	0.422	0.414
Mn^{2+}	0.015	0.016	0.016	0.016	0.013	0.015	0.015	0.012	0.015	0.015	0.008	0.015	0.016	0.016	0.016
Ca^{2+}	0.027	0.028	0.027	0.037	0.031	0.030	0.027	0.030	0.026	0.029	0.030	0.027	0.028	0.027	0.037
Mg^{2+}	1.525	1.524	1.524	1.519	1.519	1.525	1.519	1.517	1.534	1.529	1.515	1.525	1.524	1.524	1.519
Na^{+}	–	–	–	–	–	–	0.001	–	0.002	–	–	–	–	–	–
K^{+}	–	–	–	< 0.001	–	–	–	–	< 0.001	–	–	–	–	–	< 0.001
Ni^{2+}	–	–	–	–	0.002	–	0.002	–	–	–	–	–	–	–	–
Total	3.999	3.997	3.996	3.992	3.994	3.997	3.993	3.996	3.999	3.996	3.995	3.999	3.997	3.996	3.992
$Ca^{2+}+Mg^{2+}+Fe^{2+}$	1.980	1.974	1.973	1.970	1.971	1.976	1.968	1.978	1.975	1.977	1.978	1.980	1.974	1.973	1.970
mol %															
Wo	1.36	1.41	1.38	1.87	1.57	1.50	1.38	1.51	1.31	1.45	1.50	1.36	1.41	1.38	1.87
En	77.02	77.23	77.23	77.11	77.06	77.17	77.16	76.70	77.66	77.33	76.59	77.02	77.23	77.23	77.11
Fs	21.62	21.36	21.39	21.02	21.37	21.33	21.46	21.79	21.03	21.22	21.91	21.62	21.36	21.39	21.02

nd – not detected

Table 7. Chemical composition of representative high-Ca pyroxenes. Results in wt.%. Chemical formula calculated according to $6O^{2-}$

	#2	#3	#4	#6	#9	So5.ch	So6.ch	So9.	So15.	So17.	20.ch	21.ch	22.ch	25	35
SiO_2	54.14	54.12	54.26	54.17	54.29	54.31	54.08	54.40	54.39	54.36	54.14	54.12	54.26	54.17	54.29
TiO_2	0.51	0.46	0.51	0.52	0.45	0.50	0.48	0.41	0.42	0.47	0.51	0.46	0.51	0.52	0.45
Al_2O_3	0.47	0.49	0.44	0.51	0.47	0.47	0.48	0.43	0.42	0.45	0.47	0.49	0.44	0.51	0.47
V_2O_3	0.09	0.10	nd	0.02	0.04	0.05	0.03	0.05	0.04	0.06	0.09	0.10	nd	0.02	0.04
Cr_2O_3	0.82	0.87	0.75	0.98	0.83	0.72	0.84	0.82	0.81	0.78	0.82	0.87	0.75	0.98	0.83
Fe_2O_3	0.50	0.13	0.13	0.13	0.35	0.32	nd	0.16	nd	0.10	0.51	0.13	0.13	0.13	0.35
FeO	4.80	5.06	4.65	5.63	4.94	4.16	4.95	4.77	4.79	4.75	4.80	5.06	4.65	5.63	4.94
MnO	0.30	0.23	0.29	0.20	0.22	0.21	0.28	0.27	0.24	0.17	0.30	0.23	0.29	0.20	0.22
CaO	22.11	21.88	22.63	21.55	22.07	22.80	21.88	22.03	22.25	22.30	22.11	21.88	22.63	21.55	22.07
MgO	16.52	16.49	16.41	16.37	16.41	16.51	16.46	16.55	16.40	16.52	16.52	16.49	16.41	16.37	16.41
Na_2O	0.50	0.51	0.46	0.56	0.57	0.509	0.53	0.56	0.53	0.53	0.50	0.51	0.46	0.56	0.57
K_2O	nd	nd	nd	nd	nd	nd	nd	nd	nd	nd	nd	nd	nd	nd	nd
NiO	nd	0.01	nd	nd	nd	nd	nd	0.05	0.02	nd	nd	0.01	nd	nd	nd
Total	100.76	100.35	100.53	100.64	100.64	100.54	100.01	100.50	100.31	100.49	100.77	100.33	100.53	100.64	100.64
at.%															
Si^{4+}	1.973	1.979	1.980	1.978	1.980	1.979	1.983	1.984	1.987	1.983	1.974	1.979	1.980	1.978	1.980
Ti^{4+}	0.014	0.013	0.014	0.014	0.012	0.014	0.013	0.011	0.011	0.013	0.014	0.013	0.014	0.014	0.012
Al^{3+}	0.020	0.021	0.019	0.022	0.020	0.020	0.021	0.019	0.018	0.020	0.020	0.021	0.019	0.022	0.020
V^{3+}	0.003	0.003	–	0.001	0.001	0.001	0.001	0.001	0.001	0.002	0.003	0.003	–	0.001	0.001
Cr^{3+}	0.024	0.025	0.022	0.028	0.024	0.021	0.024	0.024	0.023	0.023	0.024	0.025	0.022	0.028	0.024
Fe^{3+}	0.007	0.002	0.002	0.002	0.005	0.004	–	0.002	–	0.001	0.007	0.002	0.002	0.002	0.005
Fe^{2+}	0.146	0.155	0.142	0.172	0.151	0.127	0.152	0.146	0.146	0.145	0.146	0.155	0.142	0.172	0.151
Mn^{2+}	0.009	0.007	0.009	0.006	0.007	0.007	0.009	0.008	0.007	0.005	0.009	0.007	0.009	0.006	0.007
Ca^{2+}	0.864	0.857	0.885	0.843	0.863	0.890	0.860	0.861	0.871	0.872	0.864	0.857	0.885	0.843	0.863
Mg^{2+}	0.897	0.899	0.893	0.891	0.892	0.897	0.900	0.900	0.894	0.898	0.897	0.899	0.893	0.892	0.892
Na^{+}	0.035	0.037	0.033	0.040	0.040	0.036	0.038	0.039	0.038	0.038	0.035	0.037	0.033	0.040	0.040
K^{+}	–	–	–	–	–	–	–	–	–	–	–	–	–	–	–
Ni^{2+}	–	< 0.001	–	–	–	–	–	0.002	< 0.001	–	–	< 0.001	–	–	–
Total	3.993	3.998	3.998	3.998	3.995	3.996	4.000	3.996	3.998	3.999	3.993	3.998	3.998	3.998	3.995
$Ca^{2+}+Mg^{2+}+Fe^{2+}$	1.907	1.911	1.920	1.907	1.906	1.914	1.911	1.906	1.911	1.915	1.907	1.911	1.920	1.907	1.906
mol%															
Wo	45.28	44.85	46.09	44.23	45.27	46.51	44.98	45.16	45.58	45.52	45.28	44.85	46.09	44.23	45.27
En	47.05	47.05	46.51	46.75	46.83	46.86	47.08	47.21	46.76	46.91	47.05	47.05	46.51	46.75	46.83
Fs	7.67	8.10	7.40	9.02	7.90	6.63	7.94	7.63	7.66	7.57	7.67	8.10	7.40	9.02	7.90

nd – not detected

Table 8. Chemical composition of representative olivines. Results in wt.%. Chemical formula calculated according to $4O^{2-}$

	#1	#2	#3	#4	#5	#6	#2So1.	#3So2.	#4So3.	#5So13.	#6 So19	So13.	So19.	23.ch	26.duże	27.duże	30
SiO_2	38.36	38.54	38.31	38.66	38.71	38.45	38.49	38.58	38.52	38.50	38.31	38.50	38.31	38.36	38.54	38.31	38.66
TiO_2	nd	nd	nd	0.01	0.02	0.02	nd	0.03	nd	nd	nd	nd	nd	nd	nd	nd	0.01
Al_2O_3	nd	nd	nd	nd	nd	nd	nd	nd	nd	nd	nd	nd	nd	nd	nd	nd	nd
Cr_2O_3	nd	0.03	nd	0.01	nd	0.02	nd	0.04	0.08	0.03	0.02	0.03	0.02	nd	0.03	nd	0.01
MgO	37.97	37.86	38.08	38.16	37.98	38.17	38.90	38.80	38.22	38.11	38.00	38.11	38.00	37.97	37.86	38.08	38.16
CaO	0.06	nd	nd	nd	nd	nd	nd	0.01	0.08	nd	nd	nd	nd	0.06	nd	nd	nd
MnO	0.46	0.51	0.50	0.49	0.48	0.52	0.53	0.56	0.43	0.41	0.38	0.41	0.38	0.46	0.51	0.50	0.49
FeO	22.94	23.22	23.43	23.58	23.73	23.95	23.10	22.91	23.11	23.66	23.49	23.66	23.49	22.94	23.22	23.43	23.58
NiO	nd	nd	0.06	nd	0.03	nd	nd	0.03	nd	nd	0.04	nd	0.04	nd	nd	0.06	nd
Total	99.79	100.16	100.38	100.91	100.95	101.13	101.02	100.96	100.44	100.71	100.24	100.71	100.24	99.79	100.16	100.37	100.91
at.%																	
Si^{4+}	1.003	1.005	0.999	1.002	1.003	0.997	0.995	0.997	1.001	1.000	1.000	1.000	1.000	1.003	1.005	0.999	1.002
Ti^{4+}	–	–	–	< 0.001	–	< 0.001	–	0.001	–	–	–	–	–	–	–	–	< 0.001
Al^{3+}	–	–	–	–	–	–	–	–	–	–	–	–	–	–	–	–	–
Cr^{3+}	–	0.001	–	< 0.001	–	< 0.001	–	0.001	0.002	0.001	0.001	0.001	0.001	–	0.001	–	< 0.001
Mg^{2+}	1.480	1.472	1.480	1.474	1.467	1.475	1.499	1.495	1.481	1.476	1.478	1.476	1.478	1.480	1.472	1.480	1.474
Ca^{2+}	0.002	–	–	–	–	–	–	< 0.001	0.002	–	–	–	–	0.002	–	–	–
Mn^{2+}	0.010	0.011	0.011	0.011	0.010	0.012	0.012	0.012	0.009	0.009	0.008	0.009	0.008	0.010	0.011	0.011	0.011
Fe^{2+}	0.502	0.506	0.511	0.511	0.514	0.519	0.499	0.495	0.502	0.514	0.513	0.514	0.513	0.502	0.506	0.511	0.511
Ni^{2+}	–	–	0.001	–	0.001	–	–	0.001	–	–	0.001	–	0.001	–	–	0.001	–
Total	2.997	2.995	3.001	2.998	2.996	3.003	3.005	3.002	2.998	3.000	3.000	3.000	3.000	2.997	2.995	3.001	2.998
Si^{4+}	1.339	1.342	1.331	1.336	1.339	1.328	1.324	1.329	1.336	1.334	1.333	1.334	1.333	1.339	1.342	1.331	1.336
Ti^{4+}	< 0.001	–	–	< 0.001	–	< 0.001	–	0.001	–	–	–	–	–	< 0.001	–	–	< 0.001
Al^{3+}	–	–	–	–	–	–	–	–	–	–	–	–	–	–	–	–	–
Cr^{3+}	< 0.001	0.001	–	< 0.001	–	< 0.001	–	0.001	0.002	0.001	0.001	0.001	0.001	< 0.001	0.001	–	< 0.001
Mg^{2+}	1.976	1.966	1.972	1.967	1.959	1.965	1.995	1.992	1.976	1.968	1.971	1.968	1.971	1.976	1.966	1.972	1.967
Ca^{2+}	0.002	–	–	0.000	–	< 0.001	< 0.001	< 0.001	0.003	< 0.001	–	< 0.001	–	0.002	–	–	–
Mn^{2+}	0.014	0.015	0.015	0.014	0.014	0.015	0.015	0.016	0.013	0.012	0.011	0.012	0.011	0.014	0.015	0.015	0.014
Fe^{2+}	0.670	0.676	0.681	0.682	0.687	0.692	0.665	0.660	0.670	0.685	0.683	0.685	0.683	0.670	0.676	0.681	0.682
Ni^{2+}	–	–	0.002	–	0.001	< 0.001	–	0.001	–	–	0.001	–	0.001	–	–	0.002	–
Total	4.000	4.000	4.000	4.000	4.000	4.000	4.000	4.000	4.000	4.000	4.000	4.000	4.000	4.000	4.000	4.000	4.000
$Ca^{2+} + Mg^{2+} + Fe^{2+} + Mn^{2+} + Ni^{2+}$:																	
	1.994	1.989	2.003	1.996	1.993	2.006	2.010	2.003	1.995	1.999	2.000	1.999	2.000	1.994	1.989	2.003	1.996
mol%																	
Mo	0.08	0.00	0.00	0.00	0.00	0.00	0.00	0.01	0.12	0.01	0.00	0.01	0.00	0.08	0.00	0.00	0.00
Fo	74.25	73.98	73.89	73.86	73.64	73.54	74.57	74.62	74.23	73.83	73.91	73.83	73.91	74.25	73.98	73.89	73.86
Fa	25.16	25.45	25.50	25.60	25.81	25.89	24.85	24.72	25.18	25.71	25.63	25.71	25.63	25.16	25.45	25.50	25.60
Te	0.51	0.57	0.55	0.54	0.52	0.57	0.58	0.61	0.47	0.45	0.42	0.45	0.42	0.51	0.57	0.55	0.54
Li	0.00	0.00	0.06	0.00	0.03	0.00	0.00	0.04	0.00	0.00	0.04	0.00	0.04	0.00	0.00	0.06	0.00

nd – not detected

Table 9. Chemical composition of representative plagioclases. Results in wt.%. Chemical formula calculated according to $8O^{2-}$

	#1	#2	#13	#14	#15	So10.	So11.	So12.	sk.6.	sk.7.	sk.8.	32.	33.
SiO_2	66.09	68.39	66.45	66.75	65.61	66.45	66.75	65.61	65.95	65.53	66.90	66.09	68.39
Al_2O_3	21.33	22.57	21.83	22.47	21.41	21.83	22.47	21.41	21.31	21.30	22.21	21.33	22.57
MgO	nd	0.01	0.02	nd	nd	0.02	nd	nd	nd	nd	nd	nd	0.01
CaO	2.14	2.17	2.19	2.26	2.27	2.19	2.26	2.27	2.27	2.22	2.32	2.14	2.17
FeO	0.23	0.62	0.28	0.50	0.23	0.28	0.50	0.23	nd	nd	nd	0.23	0.62
BaO	0.02	0.07	0.01	nd	nd	0.01	nd	nd	0.13	nd	nd	0.02	0.07
Na_2O	9.57	8.92	9.26	9.61	9.63	9.26	9.61	9.63	9.91	9.91	9.19	9.57	8.92
K_2O	0.88	1.03	0.96	0.90	1.16	0.96	0.90	1.16	0.83	1.01	1.36	0.88	1.02
Total	100.26	103.78	101.01	102.49	100.32	101.01	102.49	100.32	100.41	99.97	101.98	100.26	103.78
at.%													
Si^{4+}	2.902	2.897	2.894	2.872	2.887	2.894	2.872	2.887	2.896	2.891	2.888	2.902	2.897
Al^{3+}	1.104	1.127	1.120	1.139	1.111	1.120	1.139	1.111	1.103	1.108	1.130	1.104	1.127
Mg^{2+}	–	0.001	0.001	–	–	0.001	–	–	–	–	–	–	< 0.001
Ca^{2+}	0.101	0.099	0.102	0.104	0.107	0.102	0.104	0.107	0.107	0.105	0.107	0.101	0.099
Fe^{2+}	0.001	0.003	0.001	0.003	0.001	0.001	0.003	0.001	–	–	–	0.001	0.003
Ba^{2+}	< 0.001	0.001	< 0.001	–	–	< 0.001	–	–	0.002	–	–	< 0.001	< 0.001
Na^{+}	0.814	0.733	0.782	0.801	0.822	0.782	0.801	0.822	0.844	0.848	0.769	0.814	0.733
K^{+}	0.049	0.055	0.054	0.050	0.065	0.054	0.050	0.065	0.046	0.057	0.075	0.049	0.055
Total	4.971	4.916	4.955	4.969	4.994	4.955	4.969	4.994	4.998	5.008	4.969	4.971	4.916
$Ca^{2+} + Ba^{2+} + Na^{+} + K^{+}$	0.965	0.888	0.938	0.955	0.994	0.938	0.955	0.994	0.999	1.009	0.951	0.965	0.888
mol%													
Ab	84.41	82.53	83.36	83.91	82.68	83.36	83.91	82.68	84.42	83.98	80.87	84.41	82.53
Or	5.12	6.24	5.71	5.20	6.56	5.71	5.20	6.56	4.65	5.63	7.86	5.12	6.24
An	10.42	11.09	10.92	10.89	10.76	10.92	10.89	10.76	10.70	10.39	11.27	10.42	11.09
Cs	0.04	0.14	0.01	0.00	0.00	0.01	0.00	0.00	0.23	0.00	0.00	0.05	0.14

nd – not detected

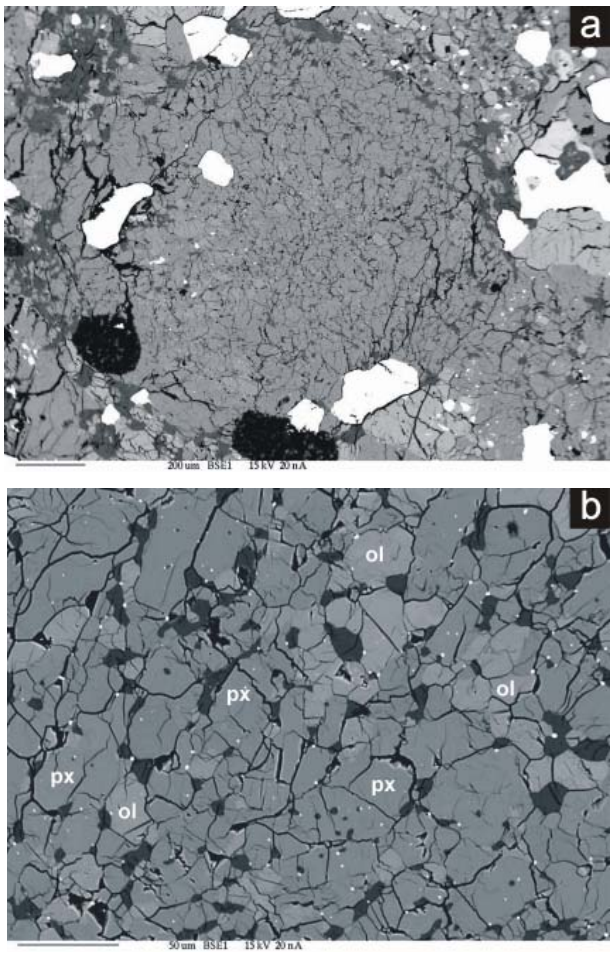

Fig. 17. Metamorphosed, recrystallized fragments of Sołtmany: **a** – rounded, fine-grained object of metamorphosed, recrystallized material, probably a former chondrule; **b** – close-up of the fine-grained interior of the object from Fig. 17a; the object is mostly composed of pyroxene (px) and (lighter in color) olivine crystals (ol); the dark spots represent grains of plagioclase. All SEM-images (BSE)

Table 10. Chemical composition of representative apatite crystals. Results in wt.%. Chemical formula calculated according to $25O^{2-}$. H_2O is calculated as a rest of the total sum of chlorine and fluorine

	#2	#3	#6
SO_3	nd	nd	0.06
P_2O_5	41.68	38.24	41.81
SiO_2	0.06	0.11	0.06
MgO	nd	nd	0.02
CaO	53.97	49.18	53.06
MnO	0.02	0.08	0.12
FeO	0.60	0.22	0.61
Na_2O	0.52	0.43	0.42
H_2O	0.56	0.33	0.72
F	nd	nd	nd
Cl	4.74	5.05	4.11
Total	102.15	93.63	100.97
at.%			
S^{6+}	–	–	0.01
P^{5+}	5.99	6.02	6.03
Si^{4+}	0.01	0.02	0.01
Mg^{2+}	–	–	0.01
Ca^{2+}	9.82	9.79	9.69
Mn^{2+}	< 0.01	0.01	0.02
Fe^{2+}	0.08	0.03	0.09
Na^{+}	0.17	0.15	0.14
OH^{-}	0.64	0.41	0.81
F^{-}	–	–	–
Cl^{-}	1.36	1.59	1.19
Total	18.09	18.03	17.99

nd – not detected

Table 11. Chemical composition of representative merrillite crystals. Results in wt.%. Chemical formula calculated according to $56O^{2-}$

	#4	#9	#10	#11	#13	#15	#16	#18
Na_2O	2.82	2.86	2.64	2.53	2.67	2.67	2.80	2.75
MgO	3.52	3.53	3.50	3.52	3.51	3.51	3.65	3.55
P_2O_5	46.80	46.43	46.32	45.82	46.52	44.61	46.35	45.63
CaO	47.29	47.05	47.16	46.77	47.16	45.10	46.46	46.81
K_2O	nd	nd	nd	nd	nd	nd	nd	nd
MnO	0.02	0.03	0.01	0.05	0.10	0.04	0.01	nd
FeO	0.81	0.63	0.51	0.52	1.02	1.03	1.03	0.62
Total	101.26	100.53	100.14	99.21	100.98	96.96	100.30	99.36
at.%								
Na^{+}	1.932	1.976	1.829	1.769	1.840	1.913	1.941	1.921
Mg^{2+}	1.857	1.874	1.866	1.895	1.858	1.935	1.945	1.912
P^{5+}	14.008	13.996	14.006	13.990	13.981	13.963	14.003	13.938
Ca^{2+}	17.914	17.950	18.049	18.073	17.939	17.867	17.767	18.097
K^{+}	–	–	–	–	–	–	–	–
Mn^{2+}	0.005	0.011	0.002	0.016	0.029	0.013	0.002	–
Fe^{2+}	0.238	0.186	0.152	0.156	0.303	0.319	0.308	0.186
Total	35.954	35.993	35.905	35.899	35.949	36.012	35.965	36.053
O	56.00	56.00	56.00	56.00	56.00	56.00	56.00	56.00

nd – not detected

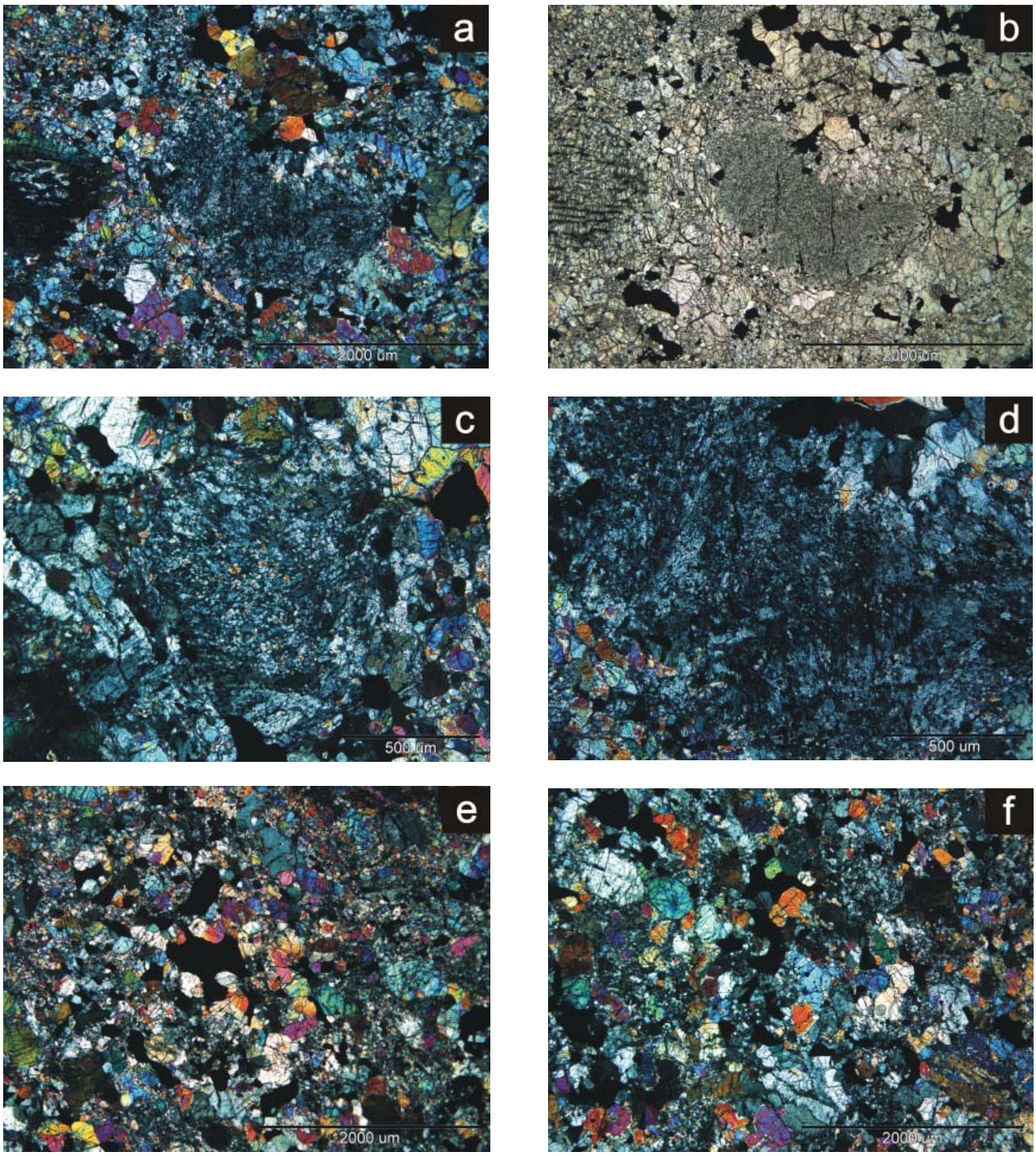

Fig. 18. Metamorphosed, recrystallized fragments in transmitted light (figs. a, c–f crossed nicols; fig. b one nicol)

Phosphates

Two phosphates, apatite and merrillite, were identified in Sołtmany. Apatite is sparse and occurs as small grains of chloro-hydroxyl apatite. The chemical composition of various apatite crystals can be found in table 10. Apatite is relatively pure in composition, as it does not contain detectable concentrations of rare earth elements (REE) and Sr. The apatite contained only a minor amount of FeO (0.5 wt.%). Merrillite is more abundant than apatite. It forms grains of significant sizes that are evenly distributed throughout the meteorite. The merrillite grains contained a significant amount of Fe. The position of Fe in the chemical structure of merrillite remains a matter of speculation. The substitution of Mg would be the most feasible position. Representative results of merrillite crystals analyses can be found in table 11.

METEORITE CLASSIFICATION AND CONCLUSION

Based upon the results of chemical analyses of pyroxenes and olivines, calculated average content of Fs in low-Ca pyroxene and olivine amounts 21.4 mol%. At the same time average Fa content in olivine equals 25.5 mol%. In accordance with the accepted classification of ordinary chondrites, Sołtmany is an L chondrite (Hutchison, 2006; McSween & Huss, 2010). Following the petrological analysis of Sołtmany, per the Van Schmus-Wood classification (1967), the chondrite is of petrologic type 6. This agrees with the observed content of Co in kamacite, which ranges between 0.75 and 0.86 at.%. Sołtmany has a weathering grade of W0 using the weathering scale developed by Wlotzka (1993). This very fresh meteorite was found within minutes following its fall and was submitted for analysis in less than a week. A shock stage of S2 was assigned to the meteorite in line with literary convention (Stöffler et al., 1991; Bischoff & Stöffler, 1992), as more than 25% of the olivine crystals exhibited undulose extinction, but planar fractures were absent.

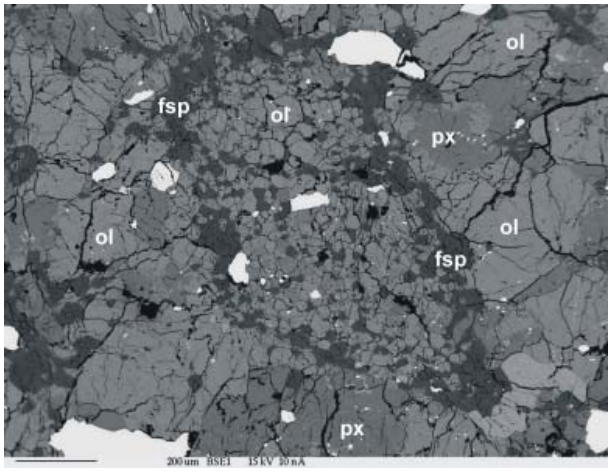

Fig. 19. Occurrence of plagioclase (fsp) around a fine-grained pyroxene (px) – olivine (ol) assemblage. SEM (BSE image)

Sołtmany is the first Polish meteorite to be thoroughly analyzed immediately after its fall. It is also the most recent chondrite of this petrologic type that was recovered shortly after having fallen in Europe. The previous fall of a similar meteorite was witnessed in April 2009 in Slovenia. However, the Jesenice L6 ordinary chondrite was not found until a few weeks after the fall, and weathering processes had already begun.

ACKNOWLEDGEMENTS

The author would like to express his gratitude to Mr. Marek Woźniak for the prompt delivery of samples, both fragments of the meteorite for thin sections, and tiny fragments of the fusion crust for analysis.

REFERENCES

Bischoff A., Stöffler D., 1992 – Shock metamorphism as a fundamental process in the evolution of planetary bodies: Information from meteorites. *European Journal of Mineralogy*, 4, 707-755.

Bischoff A., Jersek M., Grau T., Mirtic B., Ott U., Kučera J., Horstmann M., Laubenstein M., Herrmann S., Řanda Z., Weber M., Heusser G., 2011 – Jesenice – A new meteorite fall from Slovenia. *Meteoritics & Planetary Science*, 46 (6), 793-804.

Hutchison R., 2006 – Meteorites. A Petrologic, Chemical and Isotopic Synthesis. Cambridge University Press, Cambridge, UK.

McSween H.Y., Huss G.R., 2010 – Cosmochemistry. Cambridge University Press, New York, USA.

Reisener R.J., Goldstein J. I., 2003 – Ordinary chondrite metallography: Part 2. Formation of zoned and unzoned metal particles in relatively unshocked H, L, and LL chondrites. *Meteoritics & Planetary Science*, 38 (1.1), 1679-1696.

Stöffler D., Keil K., Scott E. R.D., 1991 – Shock metamorphism of ordinary chondrites. *Geochimica et Cosmochimica Acta*, 55, 3845-3867.

Van Schmus W.R., Wood J.A., 1967 – A chemical-petrologic classification for the chondritic meteorites. *Geochimica et Cosmochimica Acta*, 31, 747-765.

Wlotzka F., 1993 – A weathering scale for the ordinary chondrites. *Meteoritics*, 28, 460.

Woźniak B., Woźniak M., 2012 – Account of circumstances surrounding the fall of a meteorite in Sołtmany village. *Meteorites*, 2 (1-2), 9-14 (this number).

Publishers: Wrocław University of Technology, Faculty of Geoengineering, Mining and Geology
Polish Meteorite Society